Supplemental information

Experimental sections

1. Chemicals and materials

Bismuth nitrate ($Bi(NO_3)_3\ 5H_2O$, AR), zinc nitrate ($Zn(NO_3)_2\ 6H_2O$, AR), cetane trimethyl ammonium bromide (CTAB, AR), 2-methylimidazole (MeIM, AR), nickel nitrate hexahydrate ($Ni(NO_3)_2\ 6H_2O$, AR), concentrated hydrochloric acid (HCl), sodium hypochlorite solution (NaClO, available chlorine ≥5.0%), ammonium chloride (NH_4Cl, ≥99.99%), sodium sulfate anhydrous (Na_2SO_4, AR), potassium hydroxide (KOH, AR), sodium hydroxide (NaOH, AR), ammonium hydroxide ($NH_3\cdot H_2O$, AR), potassium bicarbonate ($KHCO_3$, AR), potassium chloride (KCl, AR), ethanol (C_2H_5OH, 99.5%), concentrated sulfuric acid (H_2SO_4), sodium salicylate ($C_7H_5O_3Na$, AR), sodium nitroprusside dihydrate ($Na_2Fe(CN)_5NO\cdot 2H_2O$, ≥98.0%), ionic strength adjuster (ISA, AR), soluble starch ($(C_6H_{10}O_5)_n$, AR), salicylic acid ($C_7H_6O_3$, AR), sodium citrate ($Na_3C_6H_5O_7$, AR), sodium sulfate anhydrous (Na_2SO_4, AR), hydrogen peroxide aqueous solution (H_2O_2, 30.0%), sodium thiosulfate pentahydrate ($Na_2S_2O_3\ 5H_2O$, AR), para-(dimethylamino) benzaldehyde ($C_9H_{11}NO$, AR), deuterium oxide (D_2O, AR), dimethyl sulfoxide (DMSO, AR), potassium iodide (KI, AR) are purchased from Sinopharma chemical reagent co. Ltd. All the reagents were used as received without further purification. Nafion 117 membrane (Dupont) was purchased from the Fuel cell store. Ultrapure water used throughout all experiments was purified through a Millipore system (Millipore, 18.2 MΩ·cm). High purity N_2 gas (≥99.999 %) and Ar (≥99.999%) gas were purchased from Shenyang Runqiao Gas Co., Ltd.

2. Electrochemical Measurements

NRR, OER and MOR electrochemical measurements were carried out by a CHI760E electrochemical workstation in a standard three-electrode set-up at room temperature. Graphite rod is used as the counter electrode, Ag/AgCl electrode or Hg/HgO electrode as the reference electrode.

NRR half-cell electrochemical measurements

The electrochemical NRR measurements were conducted in a 0.1 M $KHCO_3$ electrolyte (pH = 8.32) by using an airtight H-type cell where the cathode and anode chambers are separated by a Nafion 117 membrane. Prior to the test, Nafion 117 membranes were heat-treated in 5% H_2O_2, 0.5 M H_2SO_4, and deionized water for 1 h, respectively. After being rinsed with deionized water thoroughly, the membranes were immersed in deionized water for future use. The electrochemical measurements were performed without iR compensation.

OER and MOR half-cell electrochemical measurements

Electrochemical OER and MOR measurements were conducted in 1.0 M KOH with and without 2.0 M methanol. The linear sweep voltammetry curve (LSV) test was carried out at a scan rate of 5 mV s^{-1}. All potentials are converted to the reversible hydrogen electrode (RHE) potential ($E_{(V\ vs.\ RHE)} = E_{(V\ vs.\ Ag/AgCl)} + 0.059\ pH + 0.205$; $E_{(V\ vs.\ RHE)} = E_{(V\ vs.\ Hg/HgO)} + 0.059\ pH + 0.098$). At different scan rates of 20 to 100mV s^{-1}, the double layer capacitance (C_{dl}) value was obtained from the CV curve in the non-Faraday region. The electrochemical measurements were performed without iR compensation.

Determination of Ammonia

The quantity of the produced NH_3 was determined by indophenol blue method. Briefly, 4 mL of the post-electrolysis electrolyte was pipetted and mixed with 4 mL of 1.0 M NaOH solution with 5 wt% salicylic acid and 5 wt% sodium citrate, followed by the addition of 2 mL of 0.05 M NaClO solution and 400 μL sodium nitroferricyanide solution (1 wt%). After 1 h, the mixed solution was tested by ultraviolet-visible (UV-vis) spectrophotometer to obtain the absorption spectra. The formation of indophenol blue was determined using the absorbance at $\lambda = 655$ nm.

Ammonia quantification by ammonia-sensitive selecting electrode method. First, a series of standard ammonia solutions (0.01, 0.05, 0.1, 0.2, and 0.3 $\mu g_{NH_3}\ mL^{-1}$ in 0.1 M $KHCO_3$ and 0.01 M H_2SO_4) were prepared from a stock solution (1000 ppm ammonia) for the calibration. And the electrode slope was checked for validity (slope should be between 54 and 60 in a temperature range of 20 - 25 ℃). To minimize the impact of the background of the N_2-saturated electrolyte (0.5 M NaOH) on the quantitative analysis of the produced NH_3, each standard ammonia solution was prepared by the dilution of the stock NH_4Cl solution using the N_2-saturated 0.5 M NaOH

solution. Ionic strength adjuster (ISA) was used to provide a constant background ionic strength and adjust the pH. ISA must be added to all samples and standards immediately before measurement to prevent ammonia loss, and 80 mL of standard or sample required the addition of 1.6 mL ISA with the stirring thoroughly. In addition, the outlet gas was introduced to an acid bottle for wet scrubbing to collect the possible escaping ammonia. The ion-selective electrode meter was employed to measure the ammonia concentration in the acid wet scrubbing bottle, and the experimental results revealed that no ammonia was detected, suggesting that the ammonia escaping from the electrolyte solution is negligible.

Determination of N_2H_4

The N_2H_4 concentration was quantitatively determined by a method of Watt and Chrisp [1, 2]. To prepare a sensitive chromogenic reagent, 2.0 g para-(dimethylamino) benzaldehyde was dissolved in a mixture of 10 mL concentrated HCl and 100 mL ethanol. Then, 5 mL electrolyte was added into 5 mL coloring solution, and the adsorption spectrum was obtained by using UV-vis spectrophotometer after 15 min. The concentration of hydrazine was determined using the absorbance signal at $\lambda = 455$ nm.

Calculation of Faradaic efficiency (FE) and NH_3 yield rate

The FE for NH_3 production and NH_3 yield rate were calculated at an applied potential as follow [3]:

$$FE\ (\%) = C_{NH_3} \times V \times 3F / 17Q \quad (S1)$$

$$NH_3\ \text{yield}\ (\mu g_{NH_3}\ h^{-1}\ cm^{-2}) = C_{NH_3} \times V / (t \times A) \quad (S2)$$

where C_{NH_3} ($\mu g\ mL^{-1}$) is the concentration of NH_3, V (mL) is the volume of the electrolyte, F (96485 C mol^{-1}) is the Faraday constant, t (h) is the reduction time and A(cm^{-2}) is the mass loading of catalyst on carbon cloth, Q (C) is the quantity of applied electricity.

Calculation of Energy efficiency

The DC energy consumption of the system is calculated as follows:

Energy Consumption:

$$\text{Energy consumption (kWh dc)} = \text{Current voltage (V)} \times 1000 / (1.54 \times FE) \quad (S3)$$

Here, the constant 1.54 V is derived from the theoretical energy requirement:

$$(n \cdot F)/(3600 \cdot M_{NH_3}) = (3 \times 96485)/(3600 \times 0.017) \approx 1.54\ V \quad (S4)$$

Where n = 3 is the number of electrons transferred per mole of NH_3 , F = 96485 C mol^{-1} is the Faraday constant, M_{NH3} = 0.017 kg mol^{-1} is the molar mass of NH_3 , and the factor 3600 converts seconds to hours.

Theoretical energy consumption benchmark:

NRR system: the energy consumption consumed to produce one ton of NH_3 is 16773 kWh (9.88×10^{-4} kWh mol^{-1}_{NH3}).

NRR-MOR system: the energy consumption consumed to produce one ton of NH_3 is 30277.26 kWh (1.78×10^{-3} kWh mol^{-1}_{NH3}, 0.284 kWh mol^{-1}_{HCOOH}).

Energy Efficiency Evaluation:

The energy efficiency (%) is calculated using:

$$\text{Energy efficiency (\%)} = (\Delta H \times \Delta N)/(V \times Q) \quad \text{(S5)}$$

Where ΔH is the enthalpy change of ammonia synthesis, ΔN is the moles of ammonia produced, V is the operating voltage, and Q is the total charge passed.

The energy efficiency of NRR system is 1.25%.

The energy efficiency of NRR-MOR system is 6.30%.

Electrochemical operando ^{1}H NMR spectrum

In this experiment, the liquid phase products of methanol oxidation were detected by nuclear magnetic resonance spectroscopy. The specific test process is as follows [4]: In a typical test, 450 μL of the electrolyte after electrolysis was mixed with 50 μL of D_2O, and 0.05 μL of DMSO was added as an internal standard.

3. Calculation method

Theoretical calculations were performed using the CP2K software package based on Density Functional Theory (DFT). The electronic structure was described within the generalized gradient approximation (GGA) using the Perdew-Burke-Ernzerhof (PBE) exchange-correlation functional. The interactions between valence electrons and ionic cores were treated with the Goedecker-Teter-Hutter (GTH) norm-conserving pseudopotentials. A Gaussian and plane-wave mixed (GPW) scheme was employed, in which the Kohn-Sham orbitals were expanded using the DZVP-MOLOPT-SR basis sets, and the plane-wave cutoff energy was set to 400 eV to ensure

sufficient accuracy. To account for long-range van der Waals interactions, the Grimme DFT-D3 dispersion correction with Becke-Johnson damping (DFT-D3(BJ)) was applied.

The self-consistent field (SCF) calculations were deemed converged once the change in electronic energy between successive cycles was reduced to below 1.0×10^{-6}. All structures were fully optimized until the maximum force on each atom was below 0.02 eV $Å^{-1}$. Geometry optimizations were performed using the BFGS algorithm without imposing any symmetry constraints. A sufficiently large vacuum layer (＞15 Å) was applied along the non-periodic direction to avoid spurious interactions between periodic images. For slab models, only the Γ point was sampled due to the large supercell size.

$$E_{\text{ads}} = E_{\text{total}} - E_{\text{substrate}} - E_{\text{adsorbate}} \quad \text{(S6)}$$

Where E_{ads} is the total energy of the adsorbate-substrate system, E_{total}, $E_{\text{substrate}}$, and $E_{\text{adsorbate}}$ denote energies of the composite system, pristine substrate, and isolated adsorbate.

This computational setup has been widely validated and has been shown to accurately describe the geometric structures, electronic properties, and adsorption behaviors of defective oxides and heteroatom-doped carbon materials.

4. The techno-economical accounting (TEA) of NRR-MOR coupling electrocatalysis system:

The Faradaic efficiency was calculated according to Eq. S1

The economic performance of NRR-MOR modules can be measured by the minimum selling price (MSP) of ammonia, calculated as following:

$$MSP_{NH3} = (CAPEX \times CRF + OPEX)/m_{NH3} \quad \text{(S7)}$$

where CAPEX, the total capital expenditure, includes the capital expenditure of NRR modules and MOR modules; CRF is the return on capital on annual capital. Assuming an 8% interest rate and a 25-year product life, the CRF is 0.094; OPEX is the annual operation and maintenance cost; m_{NH3} refers to the mass of annual ammonia production, assuming that the average annual ammonia production is 1000 kg.

In the NRR-MOR coupled electrocatalytic system, additional formic acid is generated with high purity and can be commercially traded, generating additional income:

The liquid phase products of methanol oxidation were detected by nuclear magnetic resonance spectroscopy, the 450 μL electrolyte after electrolysis was quantitatively measured and determined to contain 8.5083×10^{-3} mol□L^{-1} formic acid. Assuming the average annual ammonia output is 1,000 kilograms, an additional 4910 kilograms of formic acid will be produced.

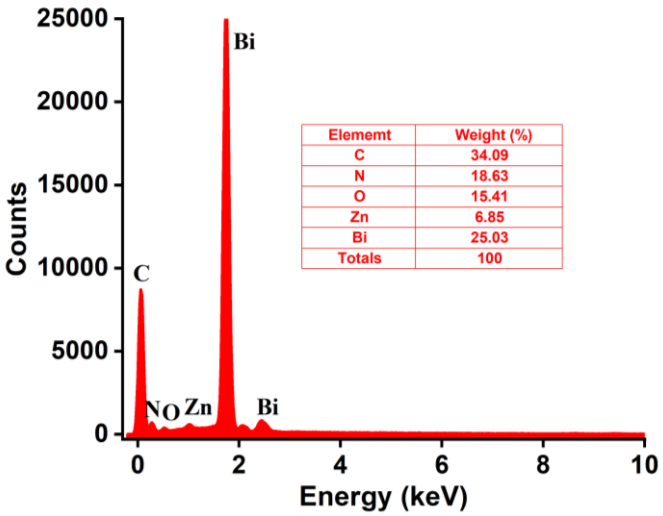

Figure S1. The EDS and corresponding mass percent of each element of Bi_2O_3/NC.

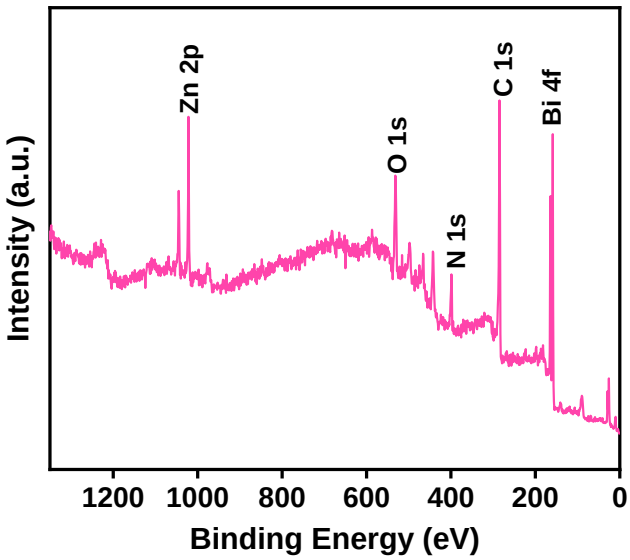

Figure S2. XPS survey spectrum of Bi_2O_3/NC.

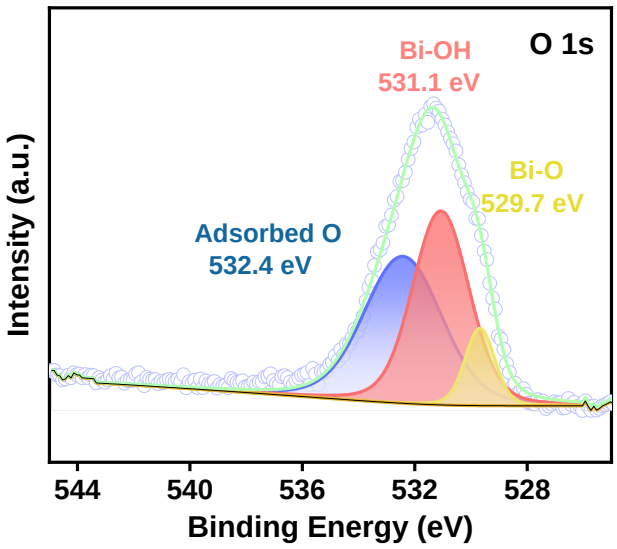

Figure S3. O 1s XPS spectrum of Bi_2O_3/NC.

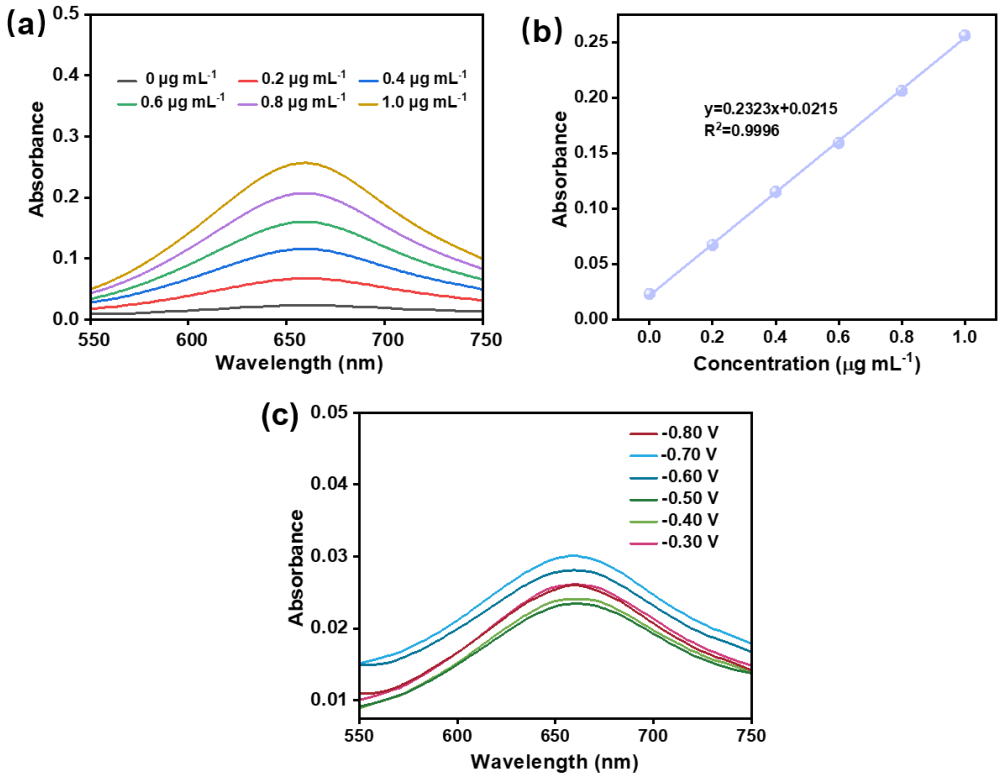

Figure S4. Determination of NH_3 in 0.1 M $KHCO_3$ electrolyte by indophenol blue method. (a) UV-vis absorption spectra of standard solutions containing different concentrations of NH_3. (b) Corresponding calibration curve. (c) UV-vis absorption spectra of each electrolyte after 2 h NRR.

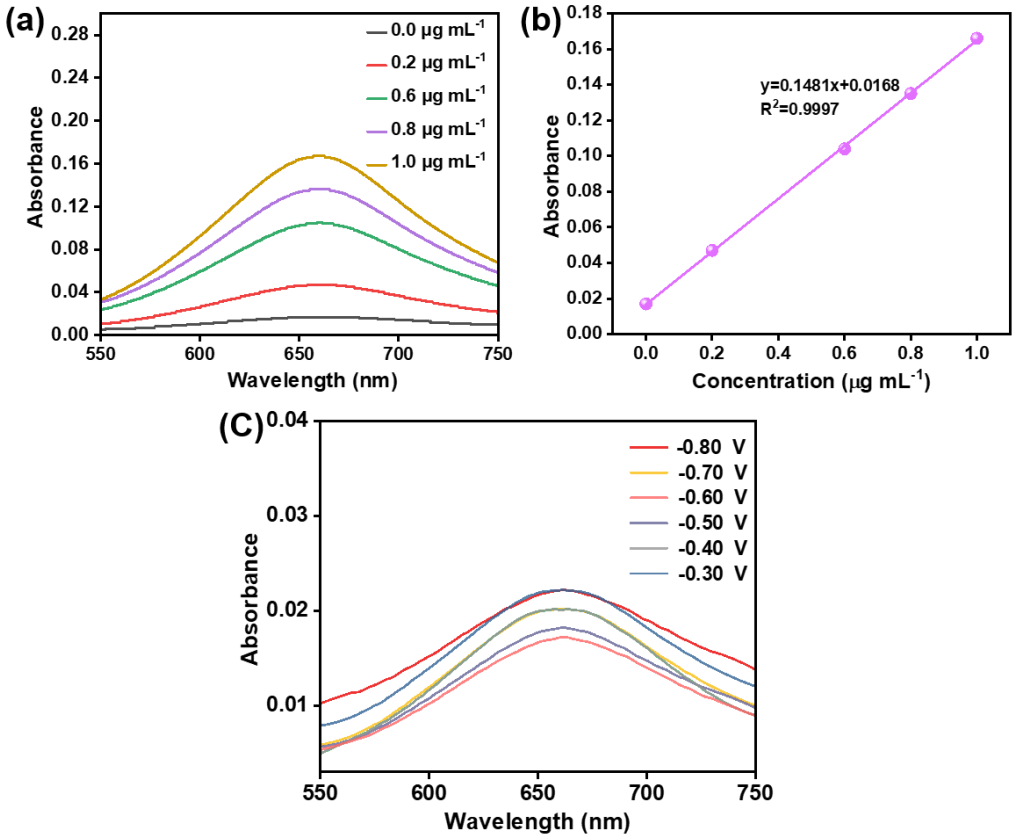

Figure S5. Determination of NH_3 in the tail gas by indophenol blue method. (a) UV-vis absorption spectra of standard solutions containing different concentrations of NH_3. (b) Corresponding calibration curve. (c) UV-vis absorption spectra of each absorption liquid after 2 h NRR.

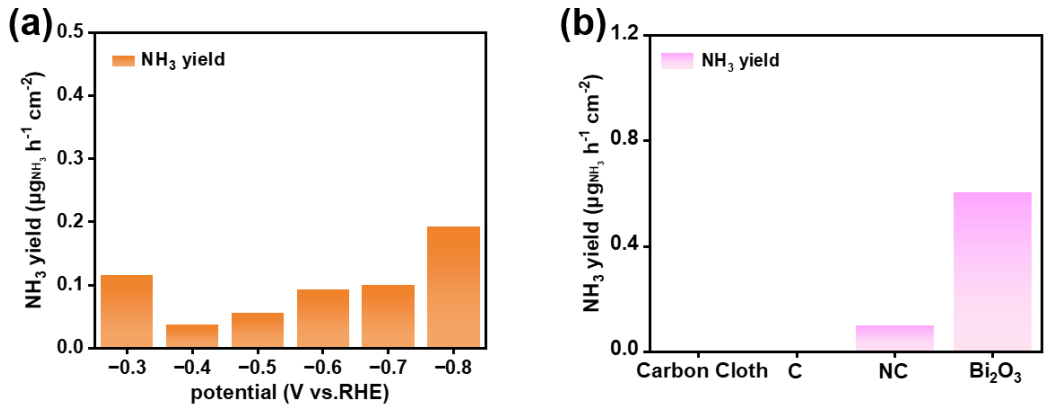

Figure S6. (a) NH_3 yields of NC at selected overpotentials, (b) NH_3 yields of carbon cloth, C, NC and Bi_2O_3 at -0.7 V vs RHE (determined by indophenol blue method).

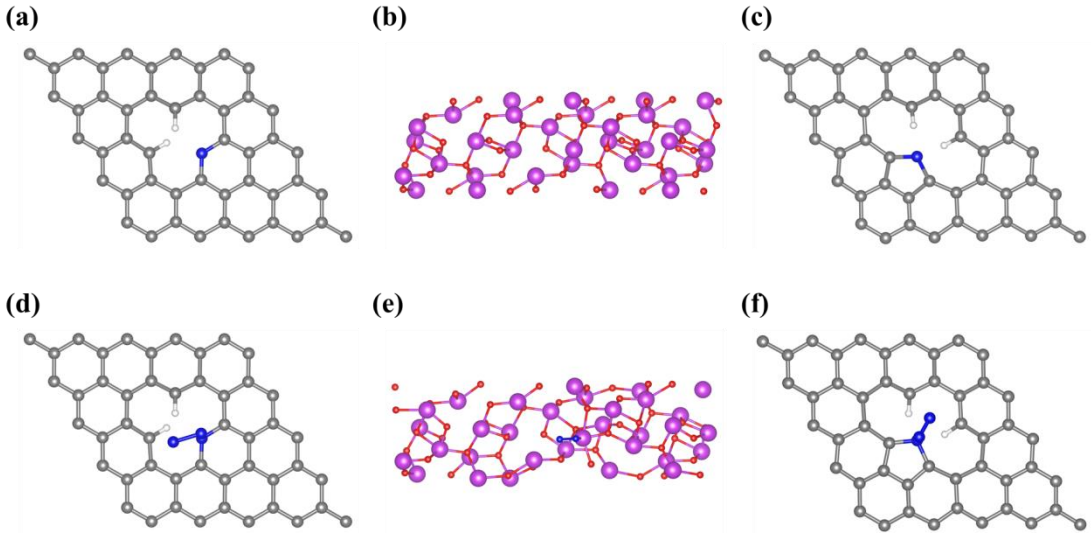

Figure S7. Optimized structures of (a) pyridinic-N-doped carbon, (b) oxygen-vacancy-rich Bi_2O_3 (203) surface, and (c) pyrrolic-N-doped carbon. Corresponding optimized configurations of N_2 adsorption on (d) pyridinic-N-doped carbon, (e) oxygen-vacancy-rich Bi_2O_3 (203) surface, and (f) pyrrolic-N-doped carbon.

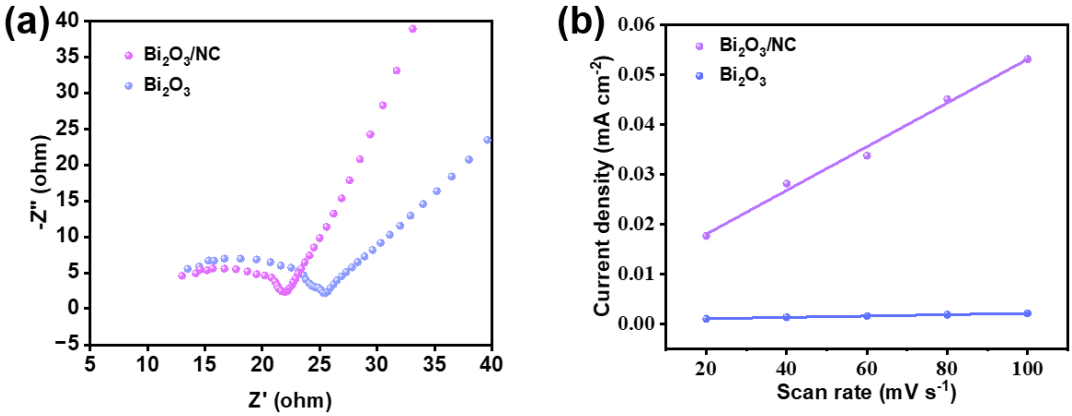

Figure S8. (a) Electrochemical impedance spectroscopies (EIS) and (b) electrochemical double-layer capacitances (Cdl) of Bi_2O_3/NC and Bi_2O_3.

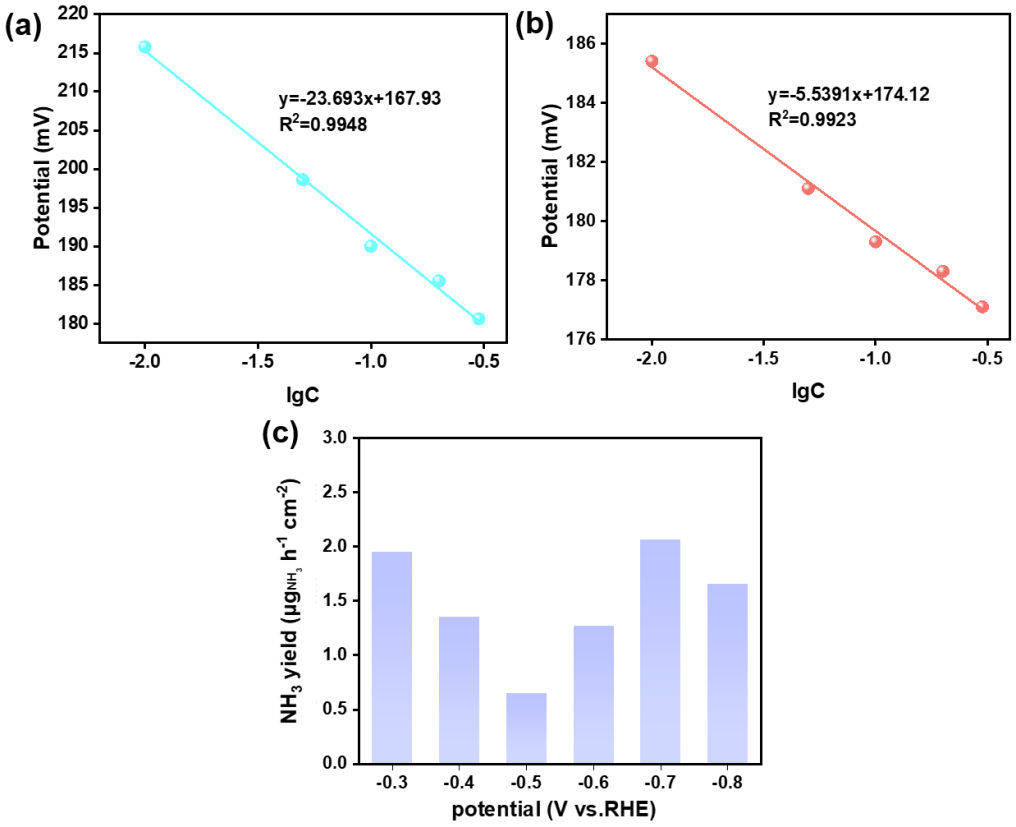

Figure S9. (a) Calibration of NH_3 with ammonia-sensitive testing instrument in 0.1 M $KHCO_3$ and (b) in 0.1 M H_2SO_4. (c) NH_3 yields of Bi_2O_3/NC at selected overpotentials determined by ammonia-sensitive testing instrument.

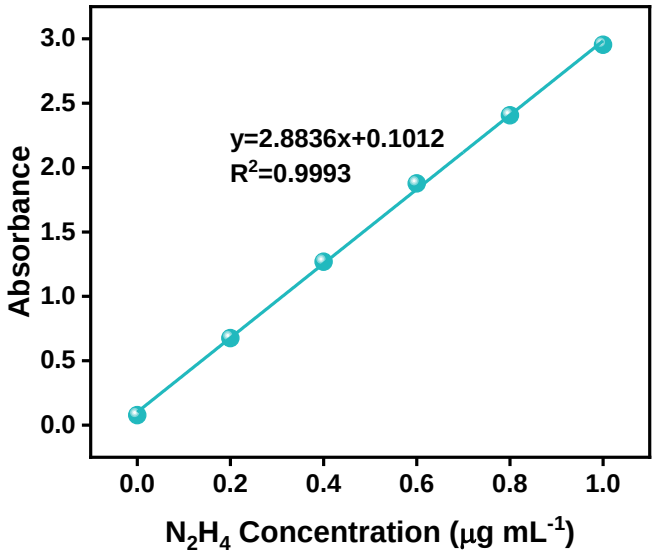

Figure S10. Calibration curve used for the estimation of the $N_2H_4 \cdot H_2O$ concentration.

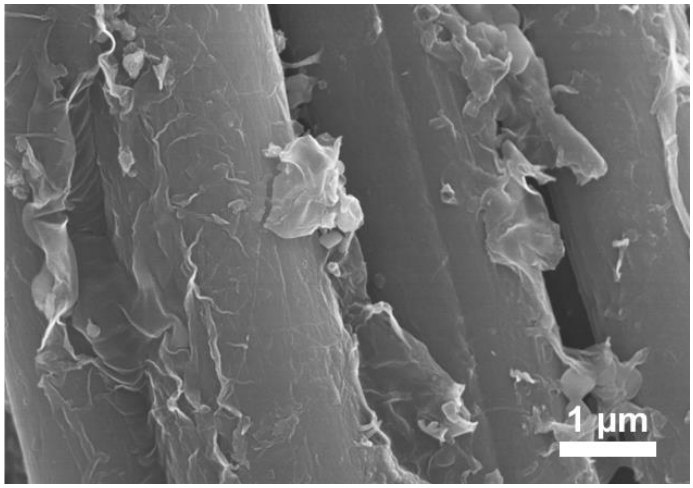

Figure S11. SEM image of Bi_2O_3/NC after NRR.

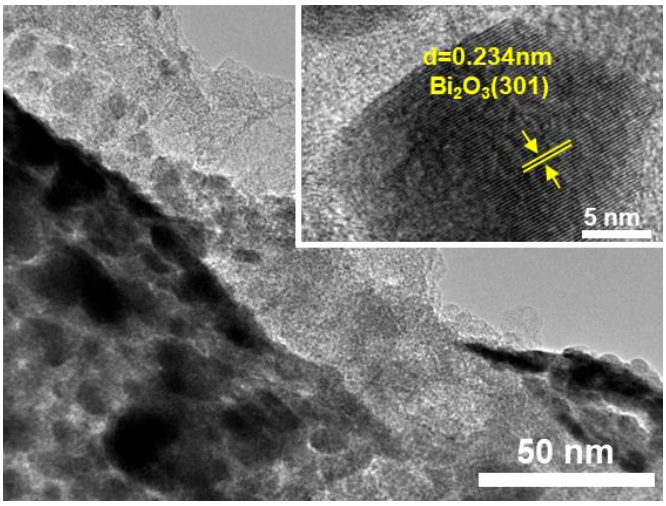

Figure S12. TEM image of Bi_2O_3/NC after NRR.

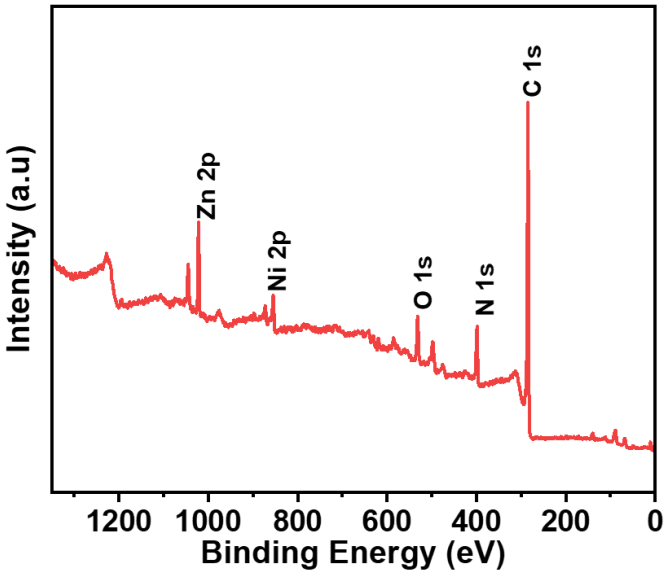

Figure S13. XPS survey spectrum of NiO/NC sample.

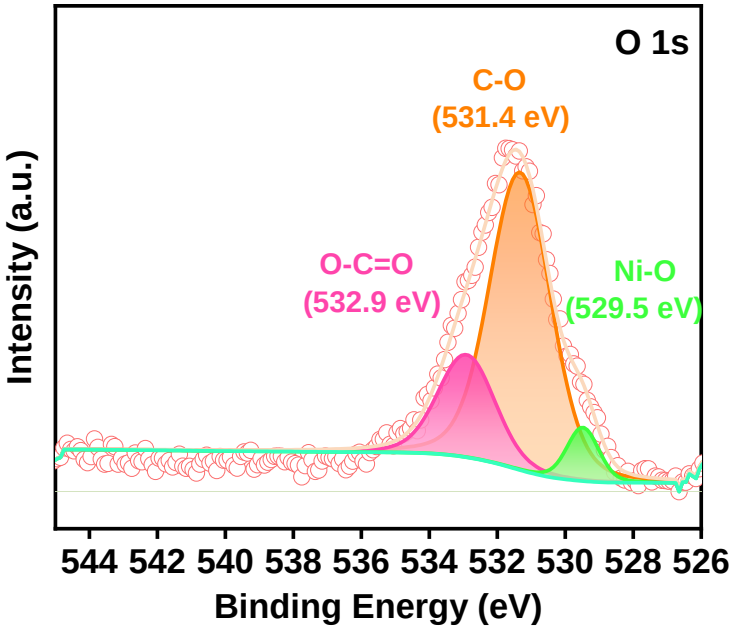

Figure S14 O1s XPS spectrum of NiO/NC.

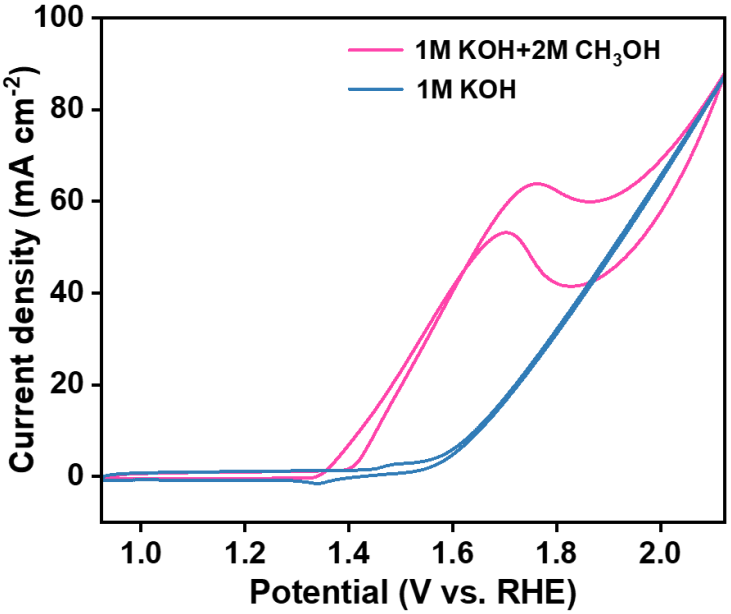

Figure S15. CV curves of NiO/NC in 1.0 M KOH with and without 2.0 M methanol at a scan rate of 100 mV s^{-1}.

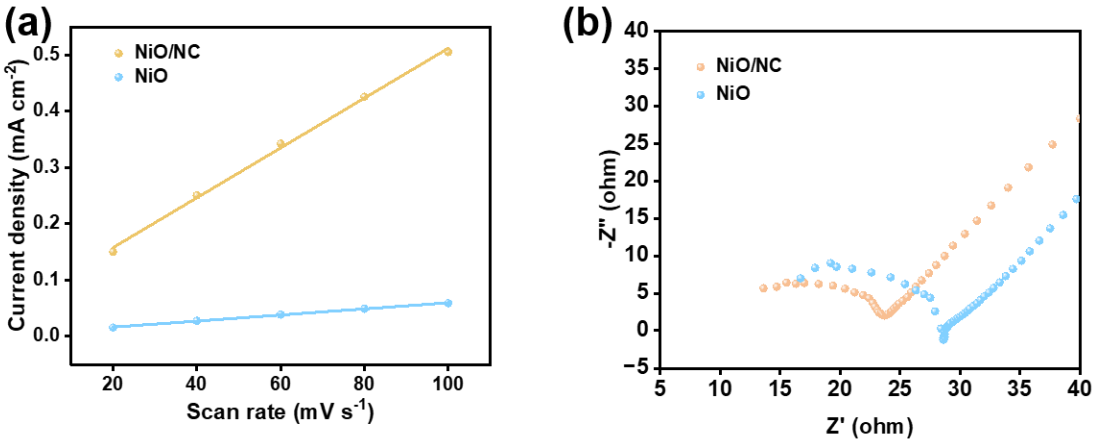

Figure S16. (a) Cdl and (b) EIS of NiO/NC and NC.

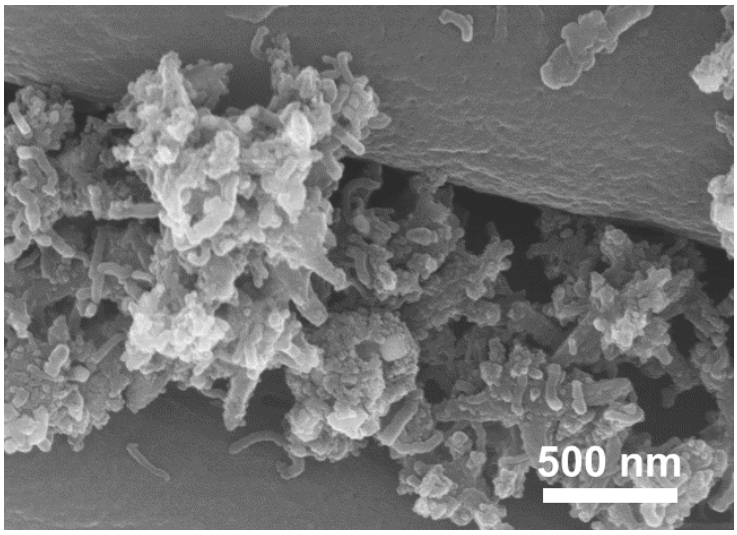

Figure S17. SEM image of NiO/NC after the anode stability test.

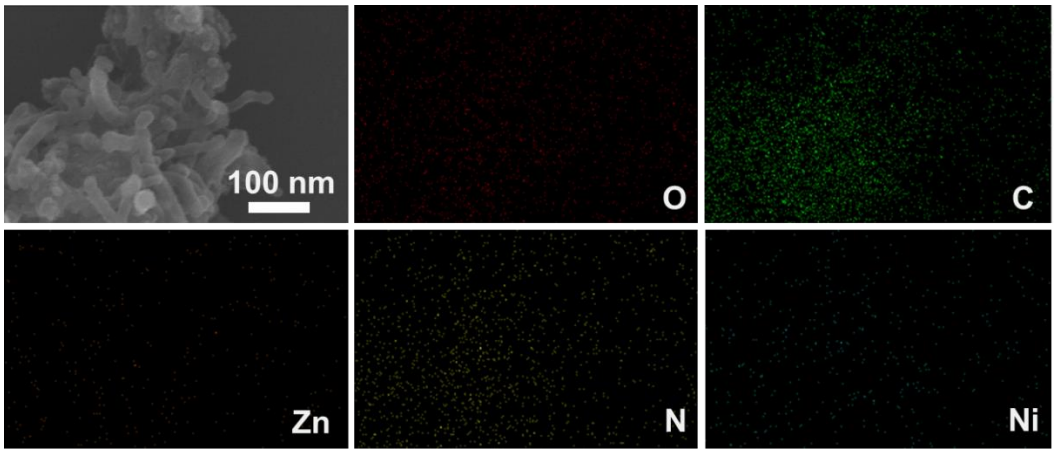

Figure S18. SEM image and EDS-mapping of NiO/NC after the anode stability test.

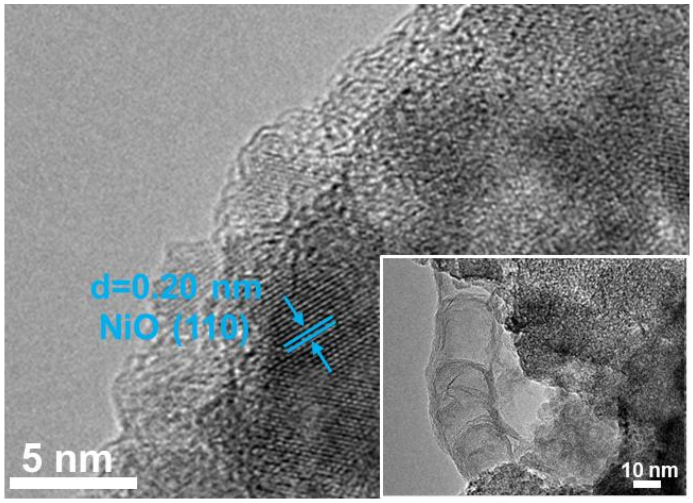

Figure S19. TEM image of NiO/NC after the anode stability test.

Table S1 Comparison of the electrocatalytic NRR performance of Bi-based with recently reported NRR electrocatalysts at room temperature.

Catalyst	Potential (*vs.* RHE)	NH_3 yield	FE	Reference
Bi_2O_3/NC	-0.7/-0.3 V	2.04 μg h^{-1} cm^{-2}	30.5%	This work
BiNs	-0.3 V	12.49 μg h^{-1} mg_{cat}^{-1}	7.09%	[5]
defect-rich Bi	-0.6 V	5.453 μg h^{-1} mg_{cat}^{-1}	11.68%	[6]
Bi@C	-0.4 V	4.22 ± 0.33 μg h^{-1} mg^{-1}	15.10 ± 0.43%	[7]
$BiVO_4$	-0.5 V	10.04 μg h^{-1} mg_{cat}^{-1}	8.6%	[8]
Bi nanodendrites	-0.6/-0.55 V	25.86 μg h^{-1} mg_{cat}^{-1}	10.8%	[9]
Sn@Ti_2CT_X/Ti_2SnC	-0.4 V	28.4 μg h^{-1} mg_{cat}^{-1}	15.57%	[10]
Sn doped $MoSe_2$@C NFMs	-0.45 V	1.61 ×10^{-10} mol s^{-1} cm^{-2}	14.51%	[11]
Bi NS	-0.4 V	1.99 μg h^{-1} mg_{cat}^{-1}	4.68%	[12]
Fe doped SnO_2	-0.8 V	28.45 μg h^{-1} mg_{cat}^{-1}	6.54%	[13]
Sn/SnS_2	-0.8 V	23.8 μg h^{-1} mg_{cat}^{-1}	3.4%	[14]
Bi/NPC	-0.6 V	3.12 μg h^{-1} cm^{-2}	13.58%	[15]
Sn_{sc}/C	-0.4 V	17.28 μg h^{-1} mg^{-1}	22.76%	[16]
Bi_2O_3/FEG	-0.5 V	4.21 ± 0.14 μg h^{-1} cm^{-2}	11.2%	[17]
BiNPs@CRs	-0.6 V	20.80 μg h^{-1} mg_{cat}^{-1}	11.50%	[18]
β-Bi_2O_3/CPE	-0.8 V	19.92 μg h^{-1} mg_{cat}^{-1}	4.3%	[19]
RuO_2-Bi_2O_3/FEG	-0.2 V	4.58 ± 0.16 μg h^{-1} cm^{-2}	14.6%	[20]
Sn ADP-0.38	-0.3 V	28.3 μg h^{-1} mg_{cat}^{-1}	26.8%	[21]
Sn D/SF	-0.6 V	5.66 ×10^{-11} mol s^{-1} cm^{-2}	23.67%	[22]
Bi NS	-0.8 V	2.54 ± 0.16 μg cm^{-2} h^{-1}	10.46 ± 1.45%	[23]
Bi-MoO_x@RGO	-0.4/-0.3 V	19.93 ± 0.47 μg h^{-1} mg_{cat}^{-1}	17.17 ± 0.81%	[24]

Table S2 Comparison of N_2 adsorption energies on pyridinic-N, pyrrolic-N, and oxygen-vacancy-containing Bi_2O_3 sites.

	Energy (a.u.)	E_{ads} (a.u.)
Pyridinic N	-283.270	
Pyridinic-N_2	-303.167	0.001
Bi_2O_3	-930.318	
Bi_2O_3-N_2	-950.221	-0.058
Pyrrolic N	-284.482	
Pyrrolic-N_2	-304.353	-0.08

Theoretical calculations indicate that both pyrrolic N and Bi are active for NRR. The adsorption energy at pyrrolic N is -0.080 a.u. (-2.17 eV), indicating a strong interaction of pyrrolic N with N_2 molecule. The oxygen-vacancy-containing Bi_2O_3 exhibits an adsorption energy of -0.058 a.u. (-1.57 eV), demonstrating stable N_2 adsorption capacity. In contrast, the pyridinic N site shows a negligible adsorption energy of 0.001 a.u. (0.027 eV), implying no adsorption capability for N_2. Defect-related Bi sites in Bi_2O_3 are thermodynamically favorable for promoting the initial adsorption and activation of N_2.

Table S3 Energy and cost analysis results.

Scenario	Content	NRR	NRR-MOR
Scenario assumptions	NH_3 yield rate ($\mu g\ h^{-1}\ cm^{-2}$)	2.04	2.79
	Energy consumption ($\$\ kW^{-1}$)	0.077	0.077
	operational cost ($\$\ kW^{-1}\ year^{-1}$)	20.00	20.00
Annual production	NH_3 production ($kg\ year^{-1}$)	1000	1000
Energy efficiency	Faradic efficiency (%)	2.71	5.04
Costs	Capital cost ($)	25305	20602
	Operational cost ($\$\ year^{-1}$)	1316	1176
MSP	Minimum selling price ($\$\ kg^{-1}_{NH_3}$)	5.06	4.97
Extra	Additional production (HCOOH, $\mu g\ h^{-1}\ cm^{-2}$)	0	1.37
	Total extraneous products ($kg\ year^{-1}$)	0	4910
	Extra income ($)	0	3314.25

Table S4 Major assumptions for economic analysis.

NH_3 production rate		1000 kg $year^{-1}$
Project lifetime		25 years
Discount rate		8%
Purchase cost		
Energy consumption		\$0.077 kW^{-1}
NRR module	Catalyst	\$200 kg^{-1}
	Carbon paper	\$1 kg^{-1}
NRR-MOR module	Catalyst	\$203 kg^{-1}
	Carbon paper	\$1 kg^{-1}
Total capital cost*		300% Purchase cost
Operation and maintenance cost		
Equipment		10% Purchase cost

*Total capital cost includes costs of purchase, installation materials (30% of purchase cost), installation labor (48% of purchase cost), insurance and tax (10% of purchase cost), construction overhead (34% of purchase cost), engineering (7% of purchase cost), contingency and fee (41% of purchase cost) and site development (30% of purchase cost). The installation and engineering costs of NRR-MOR system are assumed lower than large-scale chemical plants due to the modular system design.

Table S5 Energy and cost analysis results of NRR system.

NRR module	
Cathode	1 m^2 carbon paper + 1.0 g catalyst
Anode	1 m^2 carbon paper
Electrolyte	10 L 0.1 M $KHCO_3$
Voltage (V)	0.7
NH_3 yield (g h^{-1})	0.0204
NH_3 Faradic efficiency	2.71%
NH_3 production rate (kg $year^{-1}$)	1000
Required system electricity (kWh dc)	16772.895
Constant	Value
Faradic's canstant (C mol^{-1})	96485
Molecular weight NH_3 (g mol^{-1})	17
Electron transfer for NH_3	3
Cost analysis and NH_3 MSP	
Cost assumption	
NRR capital cost ($/NRR module)	548.3
NRR operational cost ($/NRR module/year)	11.4
Project lifetime (year)	25
Annual discount rate	8%
Annual capital recovery factor	9.40%
Cost analysis results	
NRR capital ($)	25305
NRR operational ($ $year^{-1}$)	1315
Total annualized cost ($ $year^{-1}$)	5061
NH_3 minimum selling price (MSP) ($ kg^{-1})	5.06

Table S6 Energy and cost analysis results of NRR-MOR system.

NRR-MOR module	
Cathode	1 m^2 carbon paper + 1.0 g catalyst
Anode	1 m^2 carbon paper
Electrolyte	10 L 1.0 M KOH
Voltage (V)	2.35
NH_3 yield (g h^{-1})	0.0279
NH_3 Faradic efficiency	5.04%
NH_3 production rate (kg $year^{-1}$)	1000
Required system electricity (kWh dc)	30277.26
Constant	Value
Faradic's canstant (C mol^{-1})	96485
Molecular weight NH_3 (g mol^{-1})	17
Electron transfer for NH_3	3
Cost analysis and NH_3 MSP	
Cost assumption	
capital cost ($/NRR-MOR module)	478.4
operational cost ($/NRR-MOR module/year)	9.3
Project lifetime (year)	25
Annual discount rate	8%
Annual capital recovery factor	9.40%
Cost analysis results	
NRR-MOR capital ($)	20602
NRR-MOR operational ($ $year^{-1}$)	1176
Total annualized cost ($ $year^{-1}$)	4972
NH_3 minimum selling price (MSP) ($ kg^{-1})	4.97

Table S7. Ammonia MSP for different project replacement cycles.

Replacement cycle (year)	ACRF	Additional replacement cost ($ year^{-1})	Total annualized cost ($ year^{-1})	MSP ($ kg$^{-1}_{NH_3}$)
1	1.0800	20,602	9,905	9.91
3	0.3880	6,867	6,541	6.54
5	0.2505	4,120	5,537	5.54
10	0.1490	2,060	5,112	5.11
25 (Benchmark)	0.0937	0	4,972	4.97

Table S8. Sources of parameters for techno-economic analysis.

Category	Parameter	Source
Financial	Project lifetime	Typical lifetime of chemical process plants and electrolysis systems. [25]
	Annual discount rate	Common discount rates for feasibility studies of renewable energy and chemical projects. [26]
Operational costs	Electricity price	2023 industrial average electricity price data from the U.S. EIA. [27]
Capital costs-materials	Catalyst price (NRR)	Current selling price of precursors from Sinopharma chemical reagent co. Ltd.
	Catalyst price (NRR-MOR)	Current selling price of precursors from Sinopharma chemical reagent co. Ltd.
Capital costs-installation factors	Total installed cost factor	The classic Lang factor estimation method for chemical engineering processes. [28]
	Annual maintenance cost	Typical assumptions in the technical and economic analysis of electrochemical energy systems. [25]
Technical performance	System DC-DC efficiency	Assumed efficiency for power conversion and ancillary equipment (pumps, controls). [28]
Product market	HCOOH product price	Average market price of formic acid (85% purity).

References

1. Zhang L, Ji X, Ren X, *et al*. Electrochemical ammonia synthesis via nitrogen reduction reaction on a MoS_2 catalyst: theoretical and experimental studies. Adv Mater, 2018, 30: 1800191
2. Watt GW, Chrisp JD. Spectrophotometric method for determination of hydrazine. Anal Chem, 1952, 24: 2006-2008
3. Chu K, Liu Y, Li Y, *et al*. Multi-functional Mo-doping in MnO_2 nanoflowers toward efficient and robust electrocatalytic nitrogen fixation. Appl Catal B: Environ, 2020, 264: 118525
4. Li Y, Huo C, Wang H, *et al*. Coupling CO_2 reduction with CH_3OH oxidation for efficient electrosynthesis of formate on hierarchical bifunctional CuSn alloy. Nano Energy, 2022, 98: 107277
5. Xia L, Fu W, Zhuang P, *et al*. Engineering abundant edge sites of bismuth nanosheets toward superior ambient electrocatalytic nitrogen reduction via topotactic transformation. ACS Sustain Chem Eng, 2020, 8: 2735-2741
6. Wang Y, Shi M, Bao D, *et al*. Generating defect‐rich bismuth for enhancing the rate of nitrogen electroreduction to ammonia. Angew Chem Int Ed, 2019, 131: 9564-9569
7. Wan Y, Zhou H, Zheng M, *et al*. Oxidation state modulation of bismuth for efficient electrocatalytic nitrogen reduction to ammonia. Adv Funct Mater, 2021, 31: 2100300
8. Yao J, Bao D, Zhang Q, *et al*. Tailoring oxygen vacancies of $BiVO_4$ toward highly efficient noble‐metal‐free electrocatalyst for artificial N_2 fixation under ambient conditions. Small Methods, 2019, 3: 1800333
9. Wang F, Lv X, Zhu X, *et al*. Bi nanodendrites for efficient electrocatalytic N_2 fixation to NH_3 under ambient conditions. Chem Commun, 2020, 56: 2107-2110
10. Dai X, Du Z, Sun Y, *et al*. Enhancing green ammonia electrosynthesis through tuning Sn vacancies in Sn-based MXene/MAX hybrids. Nano-Micro Lett, 2024, 16: 89
11. Huang S, Zhang M, Liu Y. In preparation and NRR application of transition metal nanosheets on carbon nanofiber membranes. J Phys Conf Ser, 2021, p 012222
12. Tu J, Li J, Pan Z, *et al*. Ultra-thin bismuth nanosheets on copper foam enabling high-efficiency electrocatalytic nitrogen reduction for ammonia synthesis. J Power Sources, 2024, 624: 235618
13. Li Y, Liu Y, Liu X, *et al*. Fe-doped SnO_2 nanosheet for ambient electrocatalytic nitrogen reduction reaction. Nano Res, 2022, 15: 6026-6035
14. Li P, Fu W, Zhuang P, *et al*. Amorphous Sn/crystalline SnS_2 nanosheets via in situ electrochemical reduction methodology for highly efficient ambient N_2 fixation. Small, 2019, 15: 1902535
15. Wu Q, Sun Y, Zhao Q, *et al*. Bismuth stabilized by ZIF derivatives for electrochemical ammonia production: proton donation effect of phosphorus dopants. Nano Res, 2022, 16: 4574-4581
16. Xue Z, Sun C, Zhao M, *et al*. Efficient electrocatalytic nitrogen reduction to ammonia on ultrafine Sn nanoparticles. ACS Appl Mater Interfaces, 2021, 13: 59834-59842
17. Sun Y, Deng Z, Song X, *et al*. Bismuth-based free-standing electrodes for ambient-condition ammonia production in neutral media. Nano-Micro Lett, 2020, 12: 1-12
18. Wang F, Zhang L, Wang T, *et al*. In situ derived Bi nanoparticles confined in carbon rods as an efficient electrocatalyst for ambient N_2 reduction to NH_3. Inorg Chem, 2021, 60: 7584-7589
19. Chang B, Liu Q, Chen N, *et al*. A flower-like bismuth oxide as an efficient, durable and selective electrocatalyst for artificial N_2 fixation in ambient condition. ChemCatChem, 2019, 11: 1884-1888
20. Wu Q, Yu B, Deng Z, *et al*. Synergy of Bi_2O_3 and RuO_2 nanocatalysts for low-overpotential and wide pH-window electrochemical ammonia synthesis. Chem Eur J, 2021, 27: 17395-17401

21. Zhang L, Zhou H, Yang X, *et al*. Boosting electroreduction kinetics of nitrogen to ammonia via atomically dispersed Sn protuberance. Angew Chem Int Ed, 2023, 135: e202217473
22. Lv X, Wang F, Du J, *et al*. Sn dendrites for electrocatalytic N_2 reduction to NH_3 under ambient conditions. Sustain Energy Fuels, 2020, 4: 4469-4472
23. Li L, Tang C, Xia B, *et al*. Two-dimensional mosaic bismuth nanosheets for highly selective ambient electrocatalytic nitrogen reduction. ACS Catal, 2019, 9: 2902-2908
24. Wan Y, Wang Z, Zheng M, *et al*. Heterogeneous crystalline-amorphous interface for boosted electrocatalytic nitrogen reduction to ammonia. J Mater Chem A, 2022, 11: 818-827
25. International renewable energy agency (IRENA). Green hydrogen cost reduction: scaling up electrolysers to meet the 1.5 ^{0} C climate goal. IRENA: Abu Dhabi, 2020
26. Glenk G, Reichelstein S. Economics of converting renewable power to hydrogen. Nat Energy, 2019, 4: 216-222
27. Zhuo Z, Du E, Zhang N, *et al*. Cost increase in the electricity supply to achieve carbon neutrality in China. Nat Commun, 2022, 13: 3172
28. Shaner M, Atwater H, Lewis N, *et al*. A comparative technoeconomic analysis of renewable hydrogen production using solar energy. Energy Environ Sci, 2016, 9: 2354-2371